Accepted for presentation in: 2023 Annual IEEE International Systems Conference (SysCon), Vancouver, Canada, April 2023.

Beam-based 6G Networked Sensing Architecture for Scalable Road Traffic Monitoring

Simon Häger, Marcus Haferkamp, and Christian Wietfeld
Communication Networks Institute (CNI), TU Dortmund University, 44227 Dortmund, Germany
E-mail: {Simon.Haeger, Marcus.Haferkamp, Christian.Wietfeld}@tu-dortmund.de

***Abstract*—The provisioning of wireless network-based sensing functionalities in the scope of 6G Joint Communication and Sensing (JCAS) is expected to be a driver for innovations and smart city-enabled services by future networks. Leveraging communication channels to acquire data on activities near network and sensing infrastructure constitutes the first step towards perceptive radio networks. Notably, the use of millimeter-wave (mmWave) frequencies is promising due to, e.g., inherent directionality and high time resolution boosting the performance of user positioning services constituting a prime example of channel-based sensing.**

In this work, we propose a novel 6G-aided networked sensing concept, mainly operating in mmWave beam space, and measuring along the inter-cell link, thereby enabling finer spatial sensory activity monitoring by the proposed radio sensing map (RSM) functions in the network. To evaluate the presented 6G-driven concept, we conduct vehicle detection and classification as a simulation-based case study underlining its high feasibility. Finally, we show the suitability of the enhancements offering new service potentials, such as recognizing a passing road user's trajectory.

***Index Terms*—6G sensing services, millimeter-wave, radio sensing maps, vehicle detection and classification, radio tomography.**

I. Introduction

In the preliminary discussions on future 6G networks, two research topics have arisen noticeably, i.e., (i) Joint Communication and Sensing (JCAS) enabling the provision of numerous sensing services as well as (ii) the widespread use of millimeter-wave (mmWave) frequencies [1]. Recent works tend to focus on radar-based sensing leveraging the mmWave spectrum. However, radio-based approaches, in which the channel serves as a sensor, represent an alternative approach that can also profit from the mmWave propagation characteristics. In the foreseen urban mmWave deployment scenarios, the advantages, as exemplified for 5G high-accuracy user positioning, are as follows: high time resolution due to the availability of broad bands, angle information due to the use of beamforming antenna arrays, reduced multipath disturbance, and ultra-dense infrastructure deployment providing numerous, most likely even line-of-sight (LOS) channels to the radio network [2].

Various other use cases, e.g., based on power and time measurements tracked over time, have been proposed in recent years for diverse applications, e.g., in the smart home context, typically leveraging wireless local area network (WLAN) signals. This has been the incentive for recent frequency-agnostic IEEE 802.11bf standardization activities, referred to by Wi-Fi sensing [3]. However, despite expected similar design goals,

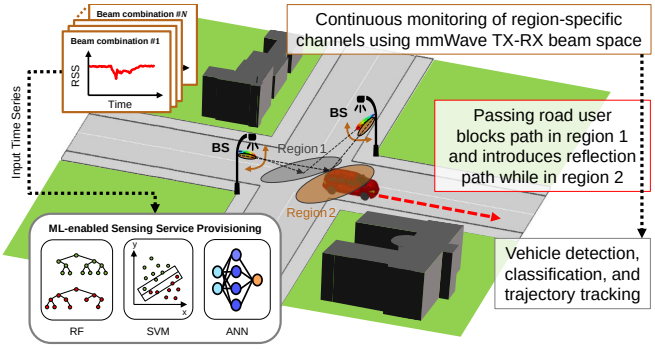

Fig. 1. Proposed 6G radio tomography system operating at mmWave carrier using beam space channelization technique along inter-cell link. This figure illustrates the applicability of ML-enabled networked sensing to an intelligent transportation system (ITS) use case in a smart city scenario.

it remains unclear which services shall be provisioned by 6G mmWave JCAS, considering the urban outdoor deployment context, which is vastly different from the local and indoor networks domain. Future cellular mmWave deployments are expected to be particularly dense in urban scenarios where high-density traffic is expected. Efficient management of vehicular traffic will be critical to solve current and future issues of the century, e.g., reducing carbon and noise emissions, introducing autonomous traffic, as well as intelligent navigation services featuring congestion avoidance and parking lot finding. With mobility covering huge distances and thus spanning larger regions, we have identified cellular networks as key enablers for both wireless connectivity and channel-based data acquisition, enabling wireless sensing services. In this work, we present a 6G system architecture for ubiquitous channel-as-a-sensor-based sensing service solutions capable of location-aware activity detection, differentiation between activity levels, and radio sensing map (RSM)-based activity tracking. We portray the proposed 6G networked sensing system with a case study for vehicle detection and classification at a street corner based on detailed ray-tracing simulations as shown in Fig. 1.

The remainder of this paper is structured as follows: Referring to related work, Sec. II provides a brief overview of the current state of research within the field of wireless sensing. Sec. III conceptualizes novel spatial sensing features for 6G networks and discusses the RSM-based activity tracking in the network core. We then conduct a case study for a vehicular application in Sec. IV to exemplify the key contributions of the proposed system. Last, we summarize this work and conclude with a brief outlook in Sec. V.

II. Related Work

As discussed previously, 6G-related research is investigating JCAS to integrate new sensing features, particularly based on the radar principle for which potential applications leveraging velocity vector, distance, angle information, and micro-Doppler/micro-range features of any nearby moving or stationary target. While the orthogonal frequency-division multiplex (OFDM) waveform of modern wireless communication systems can indeed be used for sensing, certain trade-offs between communication and sensing performance arise, e.g., caused by the signals and antenna arrays being used [4], [5]. As a result, research is investigating novel waveforms and RF front-ends which can unify both sides effectively [6], with some even proposing to design future networks entirely anew with sensing in mind [7]. Therefore, JCAS transceivers and networks will not be available for years to come. In this work, we consider communication-centric JCAS, where sensing represents a secondary use of an existing communication network requiring only minor hardware adaptions and standardization effort. Hence, it is deployable in the short-term future [6].

In contrast to radar-based sensing, services using channel-based data acquisition methods also need to be considered as modern communication technologies explicitly support these, e.g., for user positioning services [8]. To meet high-accuracy positioning service level requirements, the Third Generation Partnership Project (3GPP) recently paved the way for angle measurements on the infrastructure side [9] and simultaneous round-trip time (RTT) measurements to several base stations (BSs). This information can be leveraged in addition to key channel parameters such as signal quality, timing advance (TA), serving cell identification (C-ID), and reference signal time difference (RSTD) between cells [2]. By leveraging signals such as the positioning reference signal (PRS) from 3GPP release 16, 6G may enable multi-functional transmissions. Envisioning an open 6G system in which particularly physical (PHY) layer data is more accessible, it becomes clear that the typical control and payload signaling for the primary use of communications can be leveraged as a high-rate sensor to access frequency-dependent channel state information (CSI) continuously. For instance, this includes complex-valued channel estimates, channel impulse response (CIR) data, and Doppler shift. All of these channel parameters depend on both transmitter (TX)/receiver (RX) and ambient mobility.

Over the last decade, numerous works have resulted in a list of examples typically using WLAN-based device-to-device (D2D) communication to enable various applications and services. For example, radio-based sensing has been used for human presence and motion detection, and classification and counting of specific activities [10]. In addition, these works have sparked new standardization activities pertaining to the whole Wi-Fi spectrum, with the first major milestone having been completed in 2022 [11], whereas the first 6G standardization activities are expected to begin in 2025 at the earliest. Considering similar design targets for 6G and the growing popularity of cellular D2D communications utilizing the sidelink (SL), many of the proposed technology features and sensing-based applications are conceivable for next-generation mobile radio networks. Future 6G networks could target channel-based sensing services in ITSs due to network infrastructure availability, comprehensive coverage, and spectrum-agnostic operation.

In the vehicular context, previous works have shown that CSI acquired via WLAN and ultra-wideband (UWB) transceiver systems can be exploited by radio tomography methods to detect and classify heterogeneous road users [12], [13] characteristically affecting a system's radio link over time. Moreover, the authors in [14] further considered the importance of the used propagation paths for the sensing service, showing that sensor infrastructure does not need to be overly dense as this can result in redundancy. To put it in numbers, one to two channels suffice if these predominantly rely on propagation paths that are being temporarily disturbed by the moving road user [14]. Specifically in this work, we interpret channel disturbance events in two ways: blockage of the propagation path and creation of a new path, e.g., based on a reflection. Therefore, for 6G networked sensing it will be essential to leverage channels that target different spatial regions. In this work, we show how this may be achieved, particularly when using the well-suited mmWave spectrum, cf. Sec. I, while further unleashing novel service potentials.

III. 6G Sensing System Architecture Proposal

In this work, we propose adopting a wholesome radio-based networked sensing concept enabling flexible acquisition of channel data for location-aware activity detection as an enabler for post-detection sensing applications spanning a larger scale geographical scope. In Sec. III-A we first introduce how future networks could support channel data acquisition in a networked sensing fashion utilizing three enhancements. Afterward, we discuss how the network can use this data to become perceptive of activities in the vicinity in Sec. III-B.

A. Channels and Procedures for Data Acquisition

The classical channel-as-a-sensor approach uses a sub-6 GHz carrier between a sector antenna on the serving BS side and an omnidirectional antenna of a deployed fixed wireless access (FWA) user equipment (UE) being used either in the uplink (UL) or downlink (DL) direction. This can be extended to using both link directions and towards multiple-input multiple-output (MIMO) antenna system-based channels. Considering future multi-X connectivity, different frequency bands with measurements for several subcarriers can be considered, too. Moreover, similar to user positioning, the multi-X concept also pertains to measuring the channels to different BSs in the vicinity, further allowing for activity detection based on diverging channel behaviors. Several co-deployed UEs may also be used to create a distributed sensor field. The previously proposed techniques are depicted at the top of Fig. 2, representing the lowest level of networked sensing.

In the following paragraphs, we describe three enhancements in the scope of 6G JCAS.

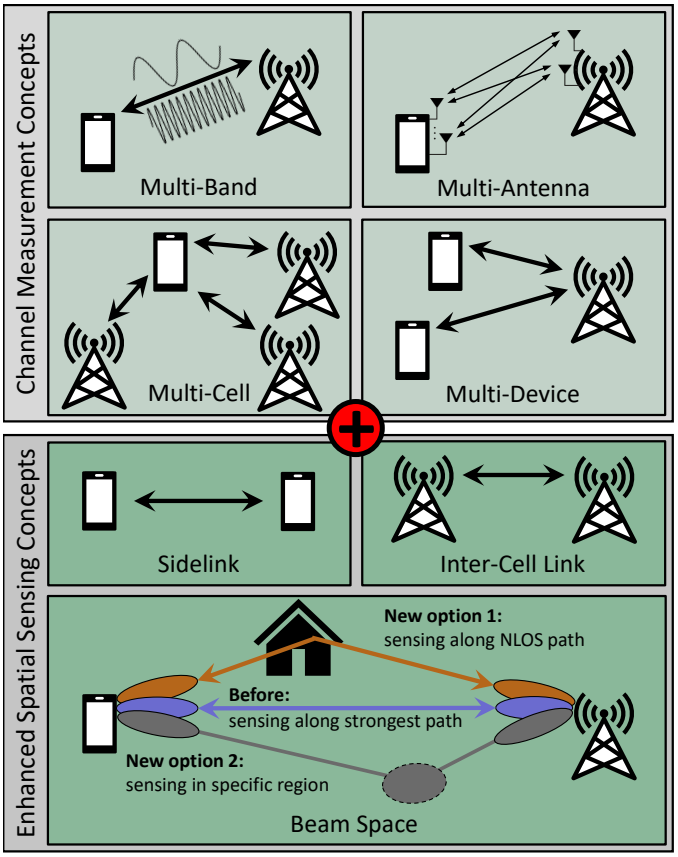

Fig. 2. Evolution: Combining concepts for 6G sensing services. *(top)* Core concepts for networked sensing using UL and DL channels. The individual measurement techniques are mutually compatible. *(bottom)* Three proposed system enhancements for fully-fledged networked sensing in 6G. Acting in beam space and using the two link types allows for spatially denser sensing.

a) Sidelink Meshing: Considering the rising interest in SL-based communication, the sensing UEs could also monitor the many D2D channels. Thus, specific regions can be closely monitored for activity depending on the deployed infrastructure and allocated spectrum resources. Moreover, assuming in-coverage SL transmissions due to the deployment of at least one sensing UE, the centralized resource allocation by the network (vehicle-to-everything (V2X) mode 3) also allows for opportunistic measurements of the channels to non-sensing UEs, e.g., of vehicles or pedestrians. Similarly, the network may leverage distinct changes in the UL channel of non-sensing UE. In some cases, this allows for a cross-check and calibration of the measurements. Alternatively, this data can also be used to filter out this event in the other measurements to focus on the privacy-preserving detection of activities due to unconnected sensing targets.

b) Operation in Beam Space: While the previously proposed sensing channels also pertain to mmWave frequencies, not all of its capabilities are yet considered. Using several BSs or UEs means that distinct propagation paths between the network and a sensor are leveraged. As illustrated in [15], there are typically several multipath opportunities that can be used deliberately for sensing services, i.e., the LOS path and several non-line-of-sight (NLOS) propagation paths. Therefore, by using different TX and RX beam combinations, e.g., in the scope of beam management procedures allowing for re-alignment of the beam along both azimuth and elevation angles on either side, the channel sensing acquires data along specific propagation paths. In case the two nodes have identified P distinct propagation paths, this allows for measuring up to P parallel channels by quickly switching through the required beam combinations. More abstractly, by assuming usage of U UE antenna beams and B BS beams, up to $U \cdot B$ channels can be measured. However, a preselection step should be considered to allow for real-time and high-rate operation using a limited number of beam combinations. Generally, the proposed radio-sensing in *beam space* thus allows for drawing conclusions about activities in certain regions in the vicinity of the available multipath between the two nodes, see at the bottom of Fig. 2 for an illustration. We note that a less directional, i.e., less mutually isolated, spatial channel sensing could also be conducted in the sub-6 GHz frequency range supporting a higher range.

c) Leveraging Inter-cell Links: Our last architecture contribution for 6G networked sensing proposes measurements along the *inter-cell link* such that, in principle, activity detection can be performed in a standalone fashion, i.e., without deployment of sensing UEs. The channel measurement may be supported by supplementary information about the original transmit signal, e.g., passed along via fiber (Xn interface), thus enabling maximum interpretability of the channel measurements. Therefore, this constitutes a bi- or multi-static networked radio-based sensing approach that mirrors concepts from the radar domain, which 6G JCAS also targets. We note that there is no use for an actual wireless link to exchange data between BSs. Still, our proposal means that inter-cell interference (ICI) turns from foe to friend, allowing one or several neighboring BSs to listen to another. Considering time-division duplex (TDD) operation, a listening BS has to prohibit UL and SL transmissions in the resources it plans to use for channel measurements. Similar resource allocation steps are also required in frequency-division duplex (FDD) mode, however, it would also be possible to reserve selected subcarriers for continuous listening to neighboring cells. Considering that there are 3GPP standardized techniques such as 5G coordinated multi-point (CoMP) transmissions and muting of resources in 5G positioning reference signals [2], network operators will not require entirely new scheduling procedures, but depending on the service requirements, a novel sensing slice may need to be introduced to the network. Considering the previous discussion, it is clear that this operation mode will reduce the network capacity as cells need to reserve resources in the time and frequency domain to listen to other BSs.

B. Local and Inter-regional Data Analysis

Using location information of facilitated BSs and sensing UEs, and possibly also additional environment maps, CSI can be mapped to distinct propagation paths in a network-internal radio sensing map (RSM). By counting the number of channels

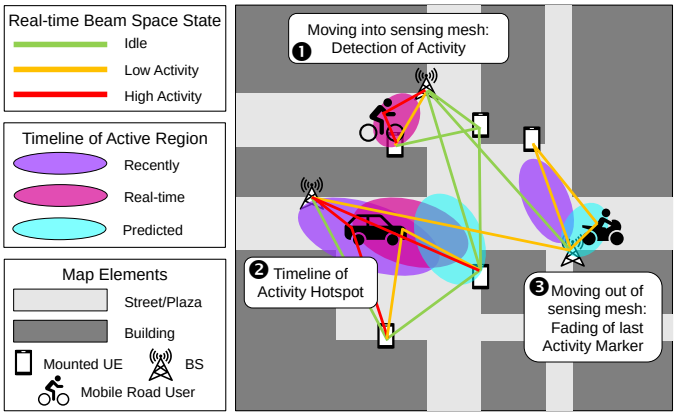

Fig. 3. Micro perspective illustration of a RSM based on a sample 6G-enabled sensing network between multiple small cells and sensing UEs.

in the same well-defined small area exhibiting a deviation from the idle state and factoring in the magnitude of the respective CSI changes (e.g., low and high), a local activity hotspot can be marked in the real-time RSM. A particular focus could lie on differentiating between the start and end of an activity and the spatial tracking thereof in terms of direction and velocity.

This overall concept is shown in Fig. 3 as follows. In step one, a cyclist impacts the channel between two nodes, thus triggering an activity detection that is projected into the RSM. Continuing along the trajectory, see step two, time-variant changes in different channels allow the network to track a vehicle's mobility. As a result, a new activity hotspot area is marked whereas the stale activity marking fades. Over longer periods of time, the marked hotspot area will follow the detected activity such that a prediction of the future activity region becomes possible based on historical data. Last, the road user leaves the coverage of the sensing mesh such that there is insufficient activity to continue the tracking. Based on the activity timeline, the network may only estimate where the activity region has moved to.

From the macro perspective, this network-internal activity map could cover the operator's coverage area (country-/campus-wide) such that multiple activities can be detected simultaneously at different places, each of which can be tracked individually. Over time, activity patterns may be detected on

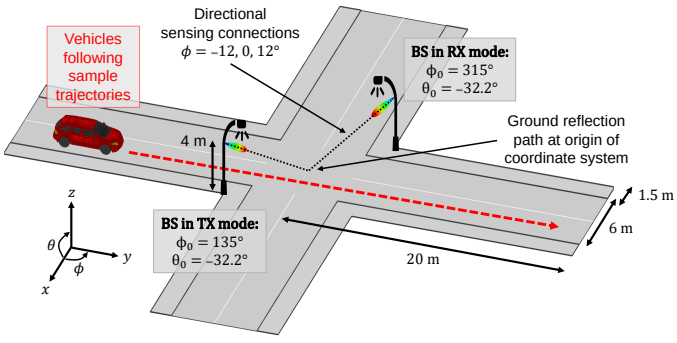

Fig. 4. Scenario of the case study. Proposed inter-cell link-based sensing enables the provision of services using only network-internal components.

a larger regional scale. Depending on infrastructure density, and utilizing transition matrices and prediction models, even outage regions can be compensated such that inter-regional activity flows can be represented wholesomely. Based on the resulting RSM, the network may optimize itself in run-time, e.g., for smoother handover and mmWave beam management. Furthermore, the RSM serves as the basis for services provided to users and third parties, e.g., city governments.

IV. Case Study of 6G Networked Sensing: Vehicular Services of Dense mmWave Deployment

In the upcoming case study, we consider 6G-enabled ITS use cases in future smart cities. For this purpose, we first describe the urban scenario together with the simulation details in Sec. IV-A. Afterward, the data preprocessing pipeline including smoothing, normalization, and feature extraction steps is explained, cf. Sec. IV-B. This is followed by Sec. IV-C briefly comparing the simulation traces to measured traces of a traditional Roadside Unit (RSU) system. Based thereon, we evaluate the proposed system's applicability regarding vehicular activity tracking and vehicle type classification as follows. In Sec. IV-D, we conduct a qualitative time series analysis for two passage scenarios emphasizing the proposed system's suitability for future real-world vehicle classification system deployments. Last, Sec. IV-E considers different trajectories to illustrate one of the emerging potentials of the proposed mmWave beam space concept for channel sensing.

A. Simulation Methodology

We consider a 40×40 m street corner scenario, as depicted in Fig. 4, with two co-deployed mmWave BSs with 4 m installation height for comprehensive coverage in all four urban canyons using a carrier frequency of 26.5 GHz.

Vehicles passing through the crossing, e.g., following the depicted trajectory along the y-axis of the Cartesian coordinate system, will affect the well-aligned directional inter-cell link, deliberately leveraging the ground reflection in the middle of the crossing. Moreover, TX and RX side pencil beams with 12° half-power beamwidth (HPBW) are swept along the azimuth angles $\phi = [-12°, 0°, 12°]$ around the respective antenna panel boresight angle tuples (ϕ_0, θ_0) following the depicted convention. Therefore, eight further distinct mmWave channels are monitored. The overall nine sensing paths thus cover different corridors in the 3D space of the crossing area. Leveraging multiple propagation paths enables the system to conduct vehicle detection and classification with improved performance, as well as newly promoted applications such as the detection of trajectory changes or the capability of handling simultaneous passages of several road users.

This work considers different vehicle passage scenarios, using eight vehicle types as summarized in Tab. I, including

- typical four- and two-wheeled vehicles (e.g., passenger car and cyclist),
- heavy-load and semi-trailer trucks, and
- pedestrians.

TABLE I
CONSIDERED FREE CAD VEHICLE MODELS.

Model Name and Source	Vehicle Classification	Dimensions ($L \times W \times H$)
Ford Edge (2008) [16]	SUV	$4.72 \times 1.93 \times 1.70$ m
VW Golf 5 GTI [16]	Car	$4.22 \times 2.08 \times 1.46$ m
Lady Snake Moto [16]	Motorbiker	$2.35 \times 0.88 \times 1.44$ m
3d Cyclist [17]	Cyclist	$1.77 \times 0.66 \times 1.85$ m
People_Man_02 [17]	Pedestrian	$0.41 \times 0.59 \times 1.80$ m
MAN [17]	Truck cab	$4.93 \times 2.49 \times 3.32$ m
Camion Volteo 8x8 [17]	Truck	$9.20 \times 2.91 \times 3.23$ m

Using these models as a baseline, we assigned different materials to the contained objects and surfaces, such as highly conductive steel (cargo area), rubber (tires, seats, clothes), and glass (windows, lamps). In contrast, the human bodies are modeled with the radio frequency (RF) characteristics of water, see Fig. 5. Using the shooting and bouncing rays (SBR+) solver of a commercial electromagnetic (EM) simulation framework [18], we simulate the different directional inter-cell channels between the two sites for each vehicle at discrete points along the trajectory as follows. We placed each vehicle in the middle of the lane and iteratively shifted the geometric center position from −7.5 m to 7.5 m after the intersecting road in uniform steps of 31.25 cm, i.e., 49 vehicle positions are traversed by the trajectory. Assuming that synchronization signals (SSs) for the mmWave cell search are exploited with a typical SS burst periodicity of 20 ms to conduct the inter-cell channel measurements at the beginning of each such burst [2], this constitutes a velocity of about 56.3 km h^{-1}. Lower velocities can be modeled by reducing the sampling rate using defined burst periodicities of up to 160 ms. In contrast, higher rate sensing with up to 200 Hz per spatial channel is also possible using these signals [2].

Further, we ran simulations not only for the trajectory which is depicted in Fig. 4 but for six in total. Fig. 6 shows the further three straight trajectories as well as two trajectories deviating from the standard trajectory by the vehicles taking a tight turn. For the right-hand turn, the three trajectories contain seven additional samples (56 in total), whereas the turn to the left results in six additional ones (55 in total). Both turns are based on trajectory planning using the Frenet reference path method with uniformly spaced simulation positions, similar to the one used for the four straight paths. Compared to the straight passages, the trajectories with a turn naturally include a vehicle rotation.

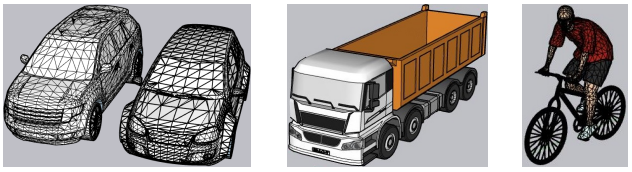

(a) SUV and car. (b) Truck. (c) Cyclist.

Fig. 5. Selection of considered road users. *(a)* Raw mesh models of passenger car and SUV. *(b)–(c)* Prepared models with realistic material assignments for simulation.

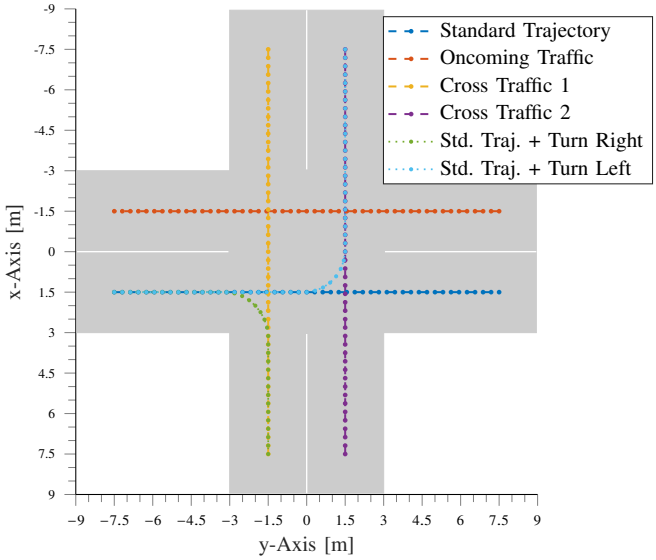

Fig. 6. Six trajectories for right-hand vehicular traffic at a street crossing used for ray-tracing-based case study.

B. Pre-processing and Evaluation of Traces

While the sensing in mmWave beam space is expected to allow for more robust vehicle type classification, operation in busy scenarios, and estimation of the overall trajectory compared to traditional RSU systems, a proper processing pipeline is critical to attain a robust activity and classification performance, using raw and high-dimensional channel data as input. In literature, multi-stage approaches combining data preprocessing (e.g., smoothing), feature extraction, and ML-based classification are widely used [12].

Fig. 1 illustrates a potential adaption of a radio-based detection and classification system utilizing two mmWave BSs, one serving as TX and the other as RX, with pencil beams closely located on a street corner. The system can perform precise road user tracking and classification by sweeping the pencil beams of either BS at a high rate for multiple beam orientations. It is worth mentioning that the proposed system design allows for an independent capturing of N region-specific channels, denoted as *region* in the figure.

Typically, the time series acquired for each beam combination serves as input for the ML-based vehicle detection and classification process, cf. Fig. 1. However, due to the small number of simulated passages for different vehicle models, we focus on the data processing and the statistical feature extraction step. First, we apply a Gaussian filter with standard deviation $\sigma = 1$ to the raw received signal strength (RSS) time series to filter the impact of signal noise. Next, we clean the smoothed time series from its absolute RSS values by transforming it to the $[0, 1]$ space using normalization (min-max-scaling). Despite being optional, the last step helps to preserve each time series's characteristics while fostering the transfer of trained ML models from a specific location to other system locations. Finally, we extract multiple statistical features from each preprocessed time series describing its

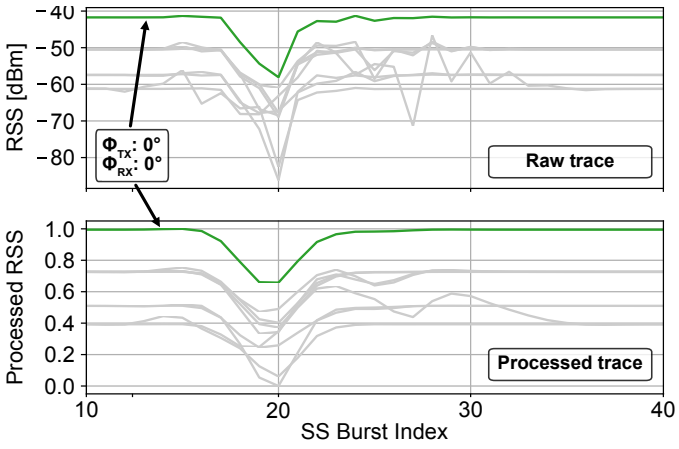

Fig. 7. *(top)* Raw and *(bottom)* post-processed mmWave traces for cyclist moving along the standard trajectory.

characteristics in a significantly compressed manner. Instead of dozens of RSS samples, we use 21 generic features for the classification task [19], thus reducing the input data dimensions. We list the long forms of the statistical feature acronyms in Tab. II. Fig. 7 illustrates the traces of all nine beam configurations acquired for a cyclist straightly passing the intersection scenario. Here, the upper subplot shows the raw time series, while the lower subplot depicts the corresponding traces after time series processing, i.e., smoothing and min-max-scaling. Subsequently, we use these processed time series for the described feature extraction.

C. Feature-based Comparison of Simulation and Real-world Measurement Traces

Before we discuss the simulation results in the following subsections, we assess the compliance of the traces gathered by the proposed simulation setup with those obtained in extensive field measurement campaigns. Specifically, we use the traces for a simulated car passage and compare them with real-world measurements utilizing a traditional RSU setup [12]. According to the previous section, we qualitatively compare the 21 derived statistical parameters from traces for a straight passage scenario, see Fig. 8.

Overall, the statistical features extracted from simulations and measurements match, thus implying that we may adapt

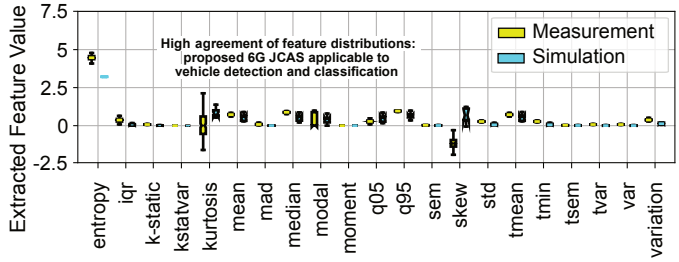

Fig. 8. Comparison of extracted features from simulation-based and real-world traces [12] for a car. The feature distributions reveal a high agreement between both methodologies justifying the proposed simulation-based evaluation.

existing detection and classification methods for sub-6 GHz radio technologies to the proposed 6G networked sensing approach. However, we note that there are some expected differences due to the different antenna mounting (elevated 6G BSs instead of RSUs) or propagation characteristics (mmWave instead of sub-6 GHz).

D. Straight Crossing Passage Scenario

First, we present the results for the simulation scenario dealing with vehicles straightly passing the road intersection along the standard trajectory, cf. Fig. 6. For the given scenario, Fig. 9a depicts the spatial RSS time series for a total of nine beam configurations along the inter-cell link resulting from different azimuth angles $\phi = [-12°, 0°, 12°]$ around angle ϕ_0 and position shifts of the vehicle passing the intersection.

Generally, the passage of the SUV impacts all nine directional channels differently, allowing one to gain certain activity information near the street crossing. For example, the ground reflection path along the center of the intersection, i.e., $(\phi_{TX}, \phi_{RX}) = (0°, 0°)$ (cf. region 1 in Fig. 1), is blocked by the vehicle resulting in a significant RSS level drop. In contrast, the channel along beam combination $(12°, -12°)$ (cf. region 2 in Fig. 1) typically manifests a low RSS due to beam misalignment. However, a passing vehicle leads to high reflection gains boosting the signal strength temporarily by more than 15 dB, which therefore indicates activity in the monitored region of the crossing.

We now compare the SUV's traces to the ones of the truck in Fig. 9b. For beam combination $(\phi_{TX}, \phi_{RX}) = (-12°, 12°)$, it can be seen that the time series differs between the vehicles: for the SUV there is first a brief gain spike followed by a descending time series whereas the truck first induces a deep fade which is afterward recovered by an ascending period. In contrast, for the $(12°, 0°)$ beam combination we find that both traces are very similar, but that the reflection and blockage-based deviations from the idle state are more pronounced for the truck. Similarly, the $(\phi_{TX}, \phi_{RX}) = (12°, -12°)$ channel time series induced by the truck exhibits a larger continuous reflection gain period in contrast to two brief bursts because of

TABLE II
ACRONYMS OF SELECTED STATISTICAL FEATURES [19].

Acronym	Long Form and Explanation
iqr	interquartile range
k-static	n-th k-static (using $n = 1$)
kstatvar	variance of k-static feature
mad	median absolute deviation
modal	most common value
moment	n-th order central moment (using $n = 2$)
q05, q95	5 %/95 % quantile
sem	standard error of the mean
std	standard deviation
tmean, tmin, tsem, tvar	trimmed mean/minimum/sem/var
var	variance
variation	coefficient of variation

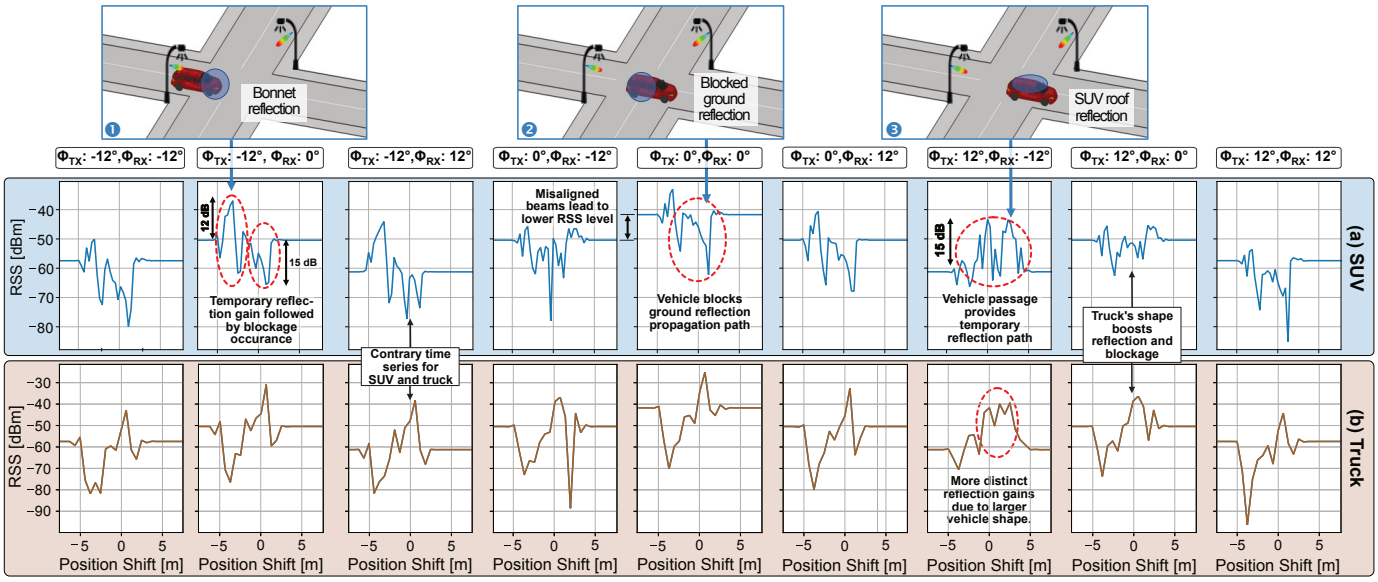

Fig. 9. Raw simulation-based mmWave beam space traces between two mmWave small cells for the passage of *(a)* SUV and *(b)* truck models. The given annotations discuss the reasons for signal gains and fades, considering the road users' shapes. Three snapshots of the SUV passage at the top illustrate the scenario state for the marked gain and fade peaks of specific beam combinations.

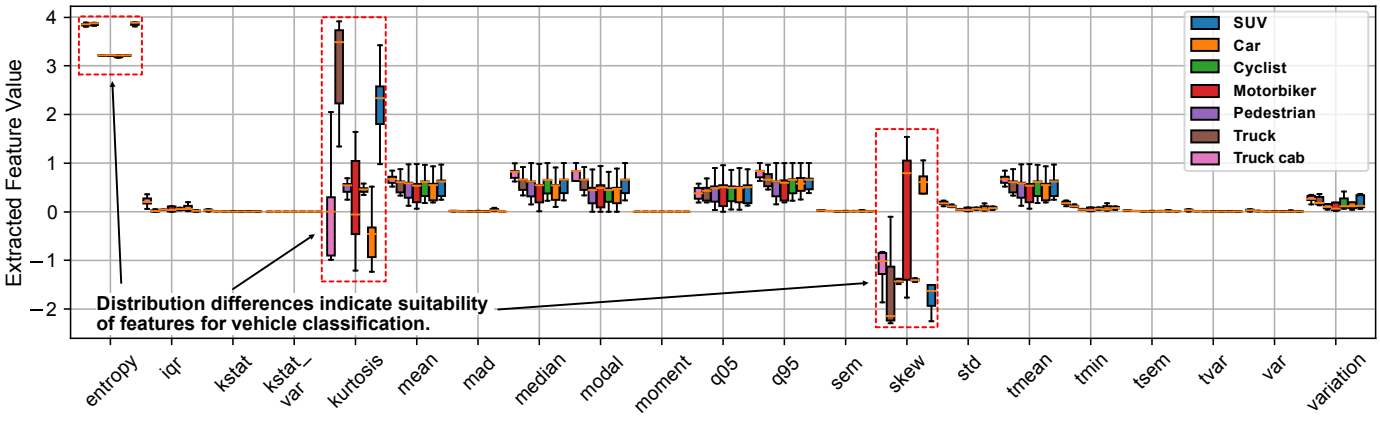

Fig. 10. Comparison of 21 statistical features (see Tab. II) between the seven vehicle models based on nine separate beam space traces.

the truck's larger shape. Moreover, when comparing the two vehicles' traces to the ones of the cyclist at the top of Fig. 7, further differences can be observed, e.g., a reduced number of reflection and blockage spikes. Therefore, we assume that the proposed system leveraging the inter-cell links in beam space will also be able to classify the vehicle types, as demonstrated in previous works focusing on sub-6 GHz radio technologies [12], [14].

Finally, we evaluate the distribution of the 21 extracted statistical features for each of the seven road users passing the intersection following the standard trajectory and each of the nine beam configurations, cf. Fig. 10. In summary, we find that the parameters *kurtosis*, *skew*, and *entropy* exhibit significantly different distribution characteristics. The previously mentioned parameters are common measures in the stochastics domain encoding information about the probability distribution of the measured passage traces. For instance, *kurtosis* describes the width of distribution (strong/weak channel distortion, i.e., vehicle shape), whereas *skew* is a measure of the asymmetry in the distribution (below/above idle state, i.e., blockage or reflection behavior). This indicates that these features may be most relevant to reduce the input data dimensions for practical road user classification.

E. Outlook: Differentiating Road User Trajectories

In this section, we briefly investigate the potential of the proposed beam space operation mode as an enabler for evolved services like mobility tracking, cf. Fig. 11. We focus on different road user trajectories, which are, for example, relevant for local governments to improve road network planning and traffic control systems.

We first compare the four straight trajectories in Fig. 8 with a particular focus on the highlighted trace using the $(\phi_{\mathrm{TX}}, \phi_{\mathrm{RX}}) = (0°, 0°)$ beam combination. It is noteworthy that the standard and oncoming passage trajectories exhibit

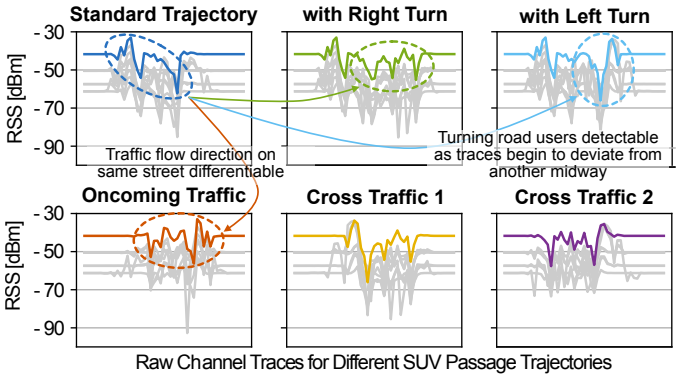

Fig. 11. Passage of SUV along four straight trajectories and two traces in which the SUV begins along the standard trajectory but turns to the right or left as depicted in Fig. 6.

different time series characteristics, similar to the two cross-traffic trajectories. Yet there are also similarities between the time series of the $(\phi_{\mathrm{TX}}, \phi_{\mathrm{RX}}) = (0°, 0°)$ beam combination, e.g., between the oncoming traffic and the two crossing trajectories. In turn, however, the gray trajectories of the eight other beam space channels differ, thus underlining the possibility of detecting different activity trajectories by considering all acquired spatial channels.

Finally, we compare the channel traces for the standard trajectory with the two trajectories in which the SUV takes a turn. Again, the number of deep attenuation fades and reflection gains differ noticeably, confirming the previous findings and, thus, underlining the high potential of this work's 6G networked sensing concept for enhanced vehicular sensing.

V. Conclusions and Future Work

This paper presented a networked sensing concept for perceptive 6G networks based on channel measurements. We proposed the adoption of data acquisition along sidelink and inter-cell link propagation paths, allowing for high-density meshed sensing compared to UL and DL measurements. Moreover, we explained the advantage of beam space channel sensing utilizing deliberate sweeping of TX and RX side mmWave antenna beams, thus enabling the monitoring of selected target regions. In this regard, we showed how network operators can leverage the radio channel to construct a location-specific radio sensing map (RSM) in the core network which is mapping and tracking activities over time and space.

In the second part of this work, we demonstrated the applicability of vehicle detection and classification for a typical urban street crossing scenario through a simulation-based case study using the proposed schemes. Furthermore, we showed that our concept enables novel services, such as differentiating between road user trajectories, which current single RSU-based systems cannot serve.

In future work, we aim to implement and evaluate the radio tomography-based vehicle detection on real traces captured with our laboratory mmWave channel sounding platform [9] taking the parallel beam space channel traces into account.

Acknowledgment

This work has received funding by the German Federal Ministry of Education and Research (BMBF) in the course of the *6GEM Research Hub* under the grant number 16KISK038. In addition, this work has been supported by the Ministry of Economic Affairs, Industry, Climate Action and Energy of the German State of North Rhine-Westphalia (MWIKE NRW) along with the *Competence Center 5G.NRW* under the grant number 005-01903-0047.

References

[1] Nokia Bell Laboratories. (2022, Jun.) Envisioning a 6G future. E-book. [Online]. Available: https://bell-labs.com/research-innovation/what-is-6g/6g-technologies (Accessed 2022-10-28).

[2] X. Lin and N. Lee, *5G and Beyond: Fundamentals and Standards*, 1st ed. Springer International Publishing, Mar. 2021.

[3] F. Restuccia, "IEEE 802.11bf: Ubiquitous Wi-Fi sensing," *arXiv cs.NI e-prints*, Mar. 2021, DOI: 10.48550/arXiv.2103.14918.

[4] A. Zhang, M. L. Rahman, X. Huang, Y. J. Guo, S. Chen, and R. W. Heath, "Perceptive mobile networks: Cellular networks with radio vision via joint communication and radar sensing," *IEEE Vehicular Technology Magazine*, vol. 16, no. 2, pp. 20–30, Sep. 2021.

[5] K. M. Braun, "OFDM radar algorithms in mobile communication networks," Ph.D. dissertation, Department of Electrical Engineering and Information Technology, Karlsruher Institute of Technology (KIT), Karslruhe, Germany, Jan. 2014.

[6] J. A. Zhang, F. Liu, C. Masouros, R. W. Heath, Z. Feng, L. Zheng, and A. Petropulu, "An overview of signal processing techniques for joint communication and radar sensing," *IEEE Journal of Selected Topics in Signal Processing*, vol. 15, no. 6, pp. 1295–1315, Nov. 2021.

[7] M. Alloulah and H. Huang, "Future millimeter-wave indoor systems: A blueprint for joint communication and sensing," *Computer*, vol. 52, no. 7, pp. 16–24, Jul. 2019.

[8] S. M. Razavi, F. Gunnarsson, H. Rydén, Å. Busin, X. Lin, X. Zhang, S. Dwivedi, I. Siomina, and R. Shreevastav, "Positioning in cellular networks: Past, present, future," in *IEEE Wireless Communications and Networking Conference (WCNC)*, Apr. 2018.

[9] K. Heimann, J. Tiemann, S. Böcker, and C. Wietfeld, "Cross–bearing based positioning as a feature of 5G millimeter wave beam alignment," in *IEEE 91st Vehicular Technology Conference (VTC-Spring)*, May 2020.

[10] Y. Ma, G. Zhou, and S. Wang, "WiFi sensing with channel state information: A survey," *ACM Computing Surveys*, vol. 52, no. 3, Jun. 2019.

[11] C. Chen, H. Song, Q. Li, F. Meneghello, F. Restuccia, and C. Cordeiro, "Wi-Fi sensing based on IEEE 802.11bf," *IEEE Communications Magazine*, vol. 61, no. 1, pp. 121–127, Jan. 2023.

[12] M. Haferkamp, B. Sliwa, and C. Wietfeld, "A low cost modular radio tomography system for bicycle and vehicle detection and classification," in *Annual IEEE International Systems Conference (SysCon)*, Apr. 2021.

[13] B. Sliwa, N. Piatkowski, and C. Wietfeld, "The channel as a traffic sensor: Vehicle detection and classification based on radio fingerprinting," *IEEE Internet of Things Journal*, vol. 7, no. 8, pp. 7392–7406, Mar. 2020.

[14] B. Sliwa, N. Piatkowski, M. Haferkamp, D. Dorn, and C. Wietfeld, "Leveraging the channel as a sensor: Real-time vehicle classification using multidimensional radio-fingerprinting," in *IEEE 21st International Conference on Intelligent Transportation Systems (ITSC)*, Nov. 2018.

[15] S. Häger, S. Böcker, and C. Wietfeld, "3D self-motion tracking services: Coalescence of mmWave beam orientations and phase information," in *IEEE Future Networks World Forum (FNWF)*, Oct. 2022.

[16] 3D CAD Browser. Free vehicle 3D models. [Online]. Available: www.3dcadbrowser.com/3dmodels.aspx?library=vehicles (Accessed 2022-10-28).

[17] Trimble Inc. 3D Warehouse: Transportation models. [Online]. Available: 3dwarehouse.sketchup.com/search/?domain=Transportation (Accessed 2022-10-28).

[18] Ansys Inc. High frequency simulation software (HFSS). [Online]. Available: www.ansys.com/hfss (Accessed 2022-10-28).

[19] SciPy documentation. Statistical functions - summary statistics. [Online]. Available: docs.scipy.org/doc/scipy/reference/stats.html?highlight=stats#summary-statistics (Accessed 2022-10-28).